FULafia Journal of Science & Technology
ISSN (print) 2449-0954 \ ISSN (online) 2636-4972
https://lafiascijournals.org.ng/index.php/fjst
Sponsored By TETFUND TERTIARY EDUCATION TRUST FUND
Manuscript => Received: Dec., 2024; Accepted: March, 2025; Published: March, 2025
https://doi.org/10.62050/fjst2025.v9n1.350

ATANGANA-BALEANU FRACTIONAL MODELING OF OLDROYD-B FLUID FLOW AND HEAT TRANSFER IN A CAPILLARY TUBE

S. M. Chimo[1,2]*, I. G. Bassi[1] and M. Abdulhameed[1,2]
[1]Department of Mathematics, Federal University of Lafia, Nasarawa State, Nigeria
[2]Department of Mathematics and Statistics, Federal Polytechnic Bauchi, Bauchi State, Nigeria
*Corresponding email: scmuhammadchimo@gmail.com

ABSTRACT
In this work, the fluid flow and heat performance of Oldroyd-B fluids, through a capillary tube, were analyzed by means of a fractional model based on the Atangana-Baleanu time-fractional derivative. The fluid motion is generated by an arbitrary pressure gradient of a continuous function of the time. Analytical solutions for the velocity and temperature fields were obtained using the Laplace transform and the finite Hankel transform. In order to obtain the physical behavior regarding the velocity and temperature at the variation of the fractional parameters, material time, pulsation frequency effect and Prandtl number we carried out numerical calculations using MathCAD software and results were graphically presented. Numerical results obtained illustrated distinct behaviors of fractional order solutions when compared with classical model solutions. The fluid velocity and heat transfer performance in capillary tube can be controlled by regulating the fractional derivative parameter, relaxation, retardation time and Prandtl number which are very important in capillary devices. This fact can be an important in Biochip technology, thus making it possible to use this analysis technique extremely effective to control bioliquid samples of nanovolumes in capillary fluidic devices used for biological analysis and medical diagnosis.

Keywords: Oldroyd-B fluid, heat transfer, Atangana-Baleanu fractional derivative, time-fractional modeling

INTRODUCTION
The non-Newtonian fluids are famous due to their diverse classical properties. With complicated nature and distinct rheology, the interest of scientists is to explore more interesting features of such materials. The nature of non-Newtonian liquids is noticed to be entirely distinct as compared to viscous liquids. The non-Newtonian liquids play one of the major contributions in various manufacturing industries, chemical processing, and engineering. The real valuable examples associated with the non-Newtonian materials are observed like starch suspension, cosmetics, molten, medicine, paints, blood, etc. The characterization of such materials is usually presented in three types like rate type, integral, and differential fluid types (Guedri *et at.*, 2022; Wang *et al.*, 2022; Veltkamp *et al.*, 2023).
Physical models of non-Newtonian fluid flow and heat transfer in terms of fractional order derivatives are fascinating subject, especially in the fields of engineering, fluid mechanics and mathematical biology. These Non-Newtonian fluid models represent more realistic behavior as compared to the integer order derivatives in fluid dynamics. This is mainly because of the freedom one gets to choose either fractional order derivatives or integer order derivatives while formulating the flow problems (Sehra *et al.*, 2023). Mathematical modeling of engineering, fluid dynamics and industrial problems usually result in the form of fractional partial differential equations. These models are controlled within their domain of validity by fractional order Partial Differential Equations PDEs. Therefore, it is imperative to be familiar with previously developed methods for solving fractional order Partial differential equations.
The theoretical interest about the flow and heat transfer characteristics of pulsating flow in closed channels is of noteworthy interest in many areas of engineering and general applications. Examples that may be given in this concept include respiratory and circulatory systems (blood flow in the main arteries and capillaries), fluid movement in biological chips used in disease diagnosis, bioreactor systems, cleaning-in-place systems, thermoacoustic systems, cooling systems of nuclear reactors and internal combustion engines along with hydraulic and pneumatic control systems (Altunkaya *et al.*, 2023).
Anwar *et al.* (2022) studied the generalized time-dependent magnetohydrodynamic (MHD) slip transport of an Oldroyd-B fluid near an oscillating upright plate. The plate was nested in a porous media under the action of ramped heating and nonlinear thermal radiation. Caputo–Fabrizio (CF) and Atangana-Baleanu (ABC) derivatives are utilized to constitute fractional partial differential equations that establish slip flow, shear stress, and heat transfer phenomena. The relations for skin friction and Nusselt number were evaluated in terms of velocity and temperature gradients to efficiently anticipate shear stress and rate of heat transfer at the solid–fluid interface. Consequently, their outcomes affirm that under the isothermal condition, a generalized Maxwell fluid performs the swiftest slip transport compared to other models. Inversely, a second

grade fluid specifies the highest velocity profile under ramped temperature case. Rathore (2023) have studied the Oldroyd-B model for biomedical purposes, which could impact medicine and health-related challenges. The comparison of Maxwell and Oldroyd-B hybrid nano models was deemed to analyze the viscoelastic nature of the blood. Altered governing equations were resolved by employing the Keller-Box scheme. Comparative results for Maxwell and Oldroyd-B models were obtained and shown graphically. The outcomes of their study show that the flow of GO-Al_2O_3 suspended blood under the Oldroyd-B model gives an improved heat transmission rate compared with the Maxwell model. Also, drug resistance was low in Oldroyd-B flow. Ali *et al.* (2024) have studied the combined influence of magnetic field, electro-osmotic flow (EOF), and pressure gradient on the unsteady magnetohydrodynamic fluid flow through a parallel microchannel. The Burger's liquid model was used for the fractional partial differential equation, which allows to study the behavior of viscoelastic liquid velocity profile in the parallel microchannel.

The Laplace transform (LT) in concert with the Fourier cosine transform were used to obtain the analytical solution of the velocity profile. Their results shows that the middle of the microchannel, fluid flow velocity increases with decrease in the delay time parameter value and increase in the Burger's parameter value, while the opposite trend is found for the velocity near to the middle of the microchannel. In addition, Burger's liquid is quite general, such that Oldroyd-B, Maxwell, and Newtonian liquids were readily obtained as limiting cases. Quran *et al.* (2024) studied the local skin friction, heating rate, and angular velocity inside boundary layer. Study's results were highlighted graphically the impact of micro polar fluid factors on the local skin friction, heating rate, and angular velocity curves were presented. The outcomes from the research show that the rising of Darcy parameter drives to decrease linearly both heating rate and local skin friction. Martín-Gil and Flores (2024) investigated the Oldroyd-B fluid flow over a permeable surface subjected to the effects of melting, slip effect, inclined magnetic field and chemical reactions. Numerical outcomes are graphically depicted by aid of velocity, concentration, temperature profiles for several model variables. Their results obtained indicated that Deborah number reduces the momentum boundary layer thickness whereas Deborah number enhances the adjacent momentum boundary layer. Zhao *et al.* (2024) analyzed the influence of Reynolds number on a velocity-vorticity correlation-based skin-friction drag decomposition in incompressible turbulent channel flows. Liu *et al.* (2024) demonstrated the correlation between skin friction and enstrophy convection velocity in near-wall turbulence. Dadheech *et al.* (2024) studied the numerical simulation for MHD Oldroyd-B fluid flow with melting and slip effect in a capillary tube. Sidahmed (2024) present the numerical study for MHD Flow of an Oldroyd-B fluid over a stretching sheet in the presence of thermal radiation with Soret and Dufour Effects.

Most of the previous studies dealt with non-Newtonian fluid flow and heat transfer over oscillating capillary are of integer order (Yin and Ma, 2013). The current study will extend the previous study using fractional order model of Atangana-Baleanu type to Model Oldroyd-B model. The aim of this paper is to derive and solved Atangana-Baleanu fluid flow and heat transfer over oscillating capillary tube.

MODELING OF THE PROBLEM

In this section, the constitutive equations governing the behaviour of Oldroyd B fluid based on Atangana-Baleanu fractional derivative will be derived. Derived model equations will be solved using Laplace transformed combined with finite Hankel transformation.

The Oldroyd-B fluid constitutive equation as in Rathore *et al.* (2023) and Sidahmed (2024) given by

$$\tau = -\mathbf{pI} + \mathbf{S} \qquad (1)$$

$$\mathbf{S} + \lambda_1 \frac{\mathrm{D}\mathbf{S}}{\mathrm{Dt}} = \mu\left(1 + \lambda_2 \frac{\mathrm{D}}{\mathrm{Dt}}\right)\mathbf{A}_1 \qquad (2)$$

where λ_1 is the relaxation time, λ_2 is the retardation time, τ is the Cauchy stress tensor, $\mathbf{S}$ is the extra stress tensor, μ is the dynamic viscosity of the fluid and $\mathbf{A}_1$ is first Rivlin Ericksen, $\mathbf{p}$ is pressure and $\mathbf{I}$ is identity matrix.

Atangana–Baleanu Fractional Differential Operator

Let $f \in H^1(a,b), b > a, \alpha \in [0,1]$ then, Atangana-Baleanu fractional derivative in Caputo and Fabrizo sense is given as

$${}^{ABC}D_t^{\alpha}\left(f(t)\right) = \frac{\mathrm{B}(\alpha)}{1-\alpha}\int_b^t \frac{df}{d\tau} E_{\alpha}\left[\frac{-\alpha(t-\tau)^{\alpha}}{1-\alpha}\right] d\tau \qquad (3)$$

whereB(α) has the same properties in Caputo and Fabrizo sense and $E_{\alpha} = \sum_{k=0}^{\infty} \frac{z^k}{\Gamma(\alpha_k+1)}$ is a Mittag-Leffler function.

Using equation (3), equations (1) and (2) becomes:

$$\tau = -\mathbf{pI} + \mathbf{S} \qquad (4)$$

$$\mathbf{S} + \lambda_1 \frac{\mathrm{D}^{\alpha}\mathbf{S}}{\mathrm{Dt}^{\alpha}} = \mu\left(1 + \lambda_2 \frac{\mathrm{D}^{\beta}}{\mathrm{Dt}^{\beta}}\right)\mathbf{A}_1 \qquad (5)$$

where α and β are the fractional parameter with $0 \le \alpha \le \beta \le 1$. For $\beta = 1$.

Momentum and Energy Equation

The momentum and energy equations govern the dynamic behaviour of fluid motion and heat transfer performance (Fati *et al.*, 2023; Dadheech *et al.*, 2024) given by

$$\rho\left(\frac{\partial \mathbf{V}}{\partial t} + \mathbf{V}.\nabla\mathbf{V}\right) = \mathrm{div}\boldsymbol{\tau} + \mathbf{F} \qquad (6)$$

$$\rho c_p\left(\frac{\partial \mathbf{T}}{\partial t} + \mathbf{V}.\nabla\mathbf{T}\right) = k\mathrm{div}\mathbf{T} + \boldsymbol{\tau}.\mathbf{L} \qquad (7)$$

where $\frac{\partial}{\partial t}$ is the material time derivative, $\nabla\mathbf{V}$ are the surface forces, $\mathbf{F}$ is the body forces, c_p is the specific heat capacity at constant pressure, k is the thermal conductivity and $\mathbf{T}$ is the temperature vector and $\mathbf{V}$ is the velocity vector.

Formulation of the Problem

Consider an incompressible, laminar, Oldroyd-B fluid pulsating flow in a capillary tube with a radius of r_0 driven by a pressure gradient that varies periodically with time as:

$$\frac{\partial p}{\partial z} = \mathbf{a_z}(A_0 + A_1\cos(\omega t)) \qquad (8)$$

where the pressure gradient contains a steady and a pulsating part, of amplitudes A_0 and A_1, respectively. The unit vector$\mathbf{a_z}$ is in the z-direction parallel to the flow, ω is the frequency of the pressure gradient and$t$ is the time. Figure 1 shows the physical geometry of the problem.

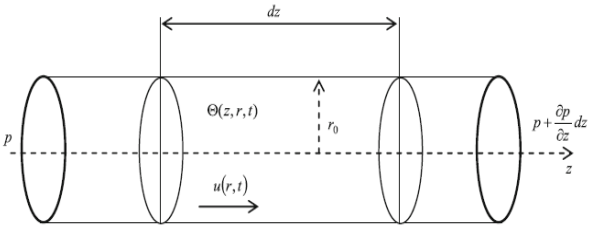

Figure 1: Physical Geometry of the problem

Figure 1 is the physical geometry of an oscillating non-Newtonian fluid flow in a round capillary tube with a radius of r_0. For the oscillating flow shown below; (i) the flow is assumed to be laminar and fully developed; (ii) the flow is incompressible; (iii) the effect of surface tension is not considered; (iv) uniform heat flow is added at the boundary and (v) the driving force added to the fluid flow is an oscillating pressure gradient.

Using equations (4), (5) and (8) in equations (6) and (7), we obtained momentum and energy equations of fractional Oldroyd-B fluid

$$\rho\left(1+\Lambda_1{}^{ABC}D_t^{\alpha}\right)\frac{\partial u}{\partial t} = -\left((A_0+A_1\cos(\omega t))\right)\left(1+\Lambda_1{}^{ABC}D_t^{\alpha}\right) + \mu\left(1+\Lambda_2{}^{ABC}D_t^{\beta}\right)\frac{1}{r}\frac{\partial}{\partial r}\left(r\frac{\partial u}{\partial r}\right) \qquad (9)$$

$$\rho c_p \Lambda_2{}^{ABC}D_t^{\alpha}T = k\frac{1}{r}\frac{\partial}{\partial r}\left(r\frac{\partial T}{\partial r}\right) + \mu\left(\frac{\partial u}{\partial r}\right) \qquad (10)$$

The initial and boundary conditions corresponding to equations (9) and (10) are:

$$u = 0 \text{ at } t = 0 \text{ for all } 0 \le r \le r_0 \qquad (11)$$

$$\frac{\partial u}{\partial r} \text{ and } \frac{\partial T}{\partial r} = 0 \text{ at } r = 0 \text{ for } t > 0 \qquad (12)$$

$$u = 0 \text{ and } T = T_w \text{ at } r = r_0 \text{ for all } t > 0 \qquad (13)$$

Consider the following dimensional variables

$$u^* = \frac{u}{u_m},\quad t^* = \frac{vt}{r_0^2},\quad r^* = \frac{r}{r_0},\quad \omega^* = \frac{\omega r_0^2}{v},\quad \Lambda_1^* = \frac{v\Lambda_1}{r_0^2},\quad \Lambda_2^* = \frac{v\Lambda_2}{r_0^2}$$

$$\gamma_0 = \frac{r_0^2}{\mu u_s}, T^* = \frac{T-T_w}{T_w}, \qquad (14)$$

Using equation (14), equations (9) to (13) have the following non-dimensional form (after dropping the * notation)

$$\left(1+\Lambda_1{}^{ABC}D_t^{\alpha}\right)\frac{\partial u}{\partial t} = -\gamma_0\left((A_0+A_1\cos(\omega t))\right)\left(1+\Lambda_1{}^{ABC}D_t^{\alpha}\right) + \left(1+\Lambda_2{}^{ABC}D_t^{\beta}\right)\frac{1}{r}\frac{\partial}{\partial r}\left(r\frac{\partial u}{\partial r}\right) \qquad (15)$$

$$Pr\,\Lambda_2{}^{ABC}D_t^{\alpha}T = k\frac{1}{r}\frac{\partial}{\partial r}\left(r\frac{\partial T}{\partial r}\right) + E_c\left(\frac{\partial u}{\partial r}\right) \qquad (16)$$

$$u = T = 0 \text{at} t = 0 \text{ for all } 0 \le r \le 1 \qquad (17)$$

$$\frac{\partial u}{\partial r} \text{ and } \frac{\partial T}{\partial r} = 0 \text{ at } r = 0 \text{ for } t > 0 \qquad (18)$$

$$u = 0 \text{ and } T = 0 \text{ at } r = 1 \text{ for all } t > 0 \qquad (19)$$

Analytical Solution of the Problem

Integral transforms

A general integral transform of the function $u(t)$ defined in the interval $a \le t \le b$ is denoted by;

$$\chi\{u(t)\} = \int_a^b S(t,s)u(t)dt \qquad (20)$$

where $S(t,s)$ is called the kernel of the transformation. The operator χ is called integral operator and s is called the transformation variable. Integral transforms have proved to be very useful in solving difference type of problems in fluid dynamics.

Laplace transformation

The Laplace transformation of a function $u(t)$ is defined by

$$\Im\{u(t)\} = \tilde{u}(s) = \int_0^{\infty} e^{-st}\,u(t)dt, \quad s > 0 \qquad (21)$$

while the inverse of Laplace transform $\Im^{-1}\{\tilde{u}(s)\}$ is given by

$$\Im^{-1}\{\tilde{u}(s)\} = u(t) = \frac{1}{2\pi i}\int_{c-i\infty}^{c+i\infty} e^{-st}\tilde{u}(s)ds, \quad s > 0 \qquad (22)$$

Laplace Transform of Atangana-Baleanu Fractional Derivatives

Let $u(r,t)$ be a velocity field, the Atangana-Baleanu fractional derivative is defined by

$${}^{ABC}\mathrm{D}_t^{\alpha}\mathrm{u}(\mathrm{r},\mathrm{t}) = \frac{\mathrm{B}(\alpha)}{1-\alpha}\int_0^{\mathrm{t}}\mathrm{E}_{\alpha}\left(-\alpha\frac{(\mathrm{t}-\tau)^{\alpha}}{1-\alpha}\right)\frac{\partial \mathrm{u}(\mathrm{r},\tau)}{\partial\tau}\mathrm{d}\tau \qquad (23)$$

The Laplace transform of equation (63) is given by

$$\Im\left\{{}^{\mathrm{ABC}}\mathrm{D}_t^{\alpha}\mathrm{u}(\mathrm{r},\mathrm{t})\right\} = \frac{s^{\alpha}\Im\{u(r,t)\}-s^{\alpha-1}u(r,0)}{s^{\alpha}(1-\alpha)+\alpha} \qquad (24)$$

Where s denotes the Laplace transform variable.

Bessel transformation (finite Hankel transformation)

The Bessel transformation or finite Hankel transformation is a generalization of the Fourier transformation

Let $u(r)$ be a function defined for $0 \le r \le 1$ that is a continuous function. The Bessel transform is defined as

$$H\{u(r)\} = \tilde{u}(\gamma_n) = \int_0^1 r\,u(r)J_0(\gamma_n r)dr \qquad (25)$$

Where J_0 is the zero-order Bessel function of the first kind and $\gamma_n, n = 1,2,\ldots,$ are the positives of the equation $J_0(\gamma_n) = 0$

The inverse Bessel transform $H^{-1}\{\tilde{u}(\gamma_n)\}$ is given by

$$H^{-1}\{\tilde{u}(\gamma_n)\} = u(r) = 2\sum_{n=1}^{\infty}\frac{\tilde{u}(\gamma_n)}{J_{n+1}^2(\gamma_n)}J_0(\gamma_n r) \qquad (26)$$

Solutions for fractional Oldroyd-B fluid flow and heat transfer

Applying the Laplace transform (23) to equations (15)-(19) and using the initial condition (17), we obtained the following transformed differential equations

$$s\bar{u}(r,s)+\frac{\lambda_1 s^{\alpha+1}\bar{u}(r,s)}{s^{\alpha}(1-\alpha)+\alpha}-\bar{F}(s)-\lambda_1\frac{s^{\alpha}F(s)-s^{\alpha-1}f(0)}{s^{\alpha}(1-\alpha)+\alpha}+\left[1+\frac{\lambda_2 s^{\beta}}{s^{\beta}(1-\beta)+\beta}\right]\frac{1}{r}\frac{\partial}{\partial r}\left(r\frac{\partial\bar{u}(r,s)}{\partial r}\right) \quad (27)$$

$$\frac{Pr\lambda_1 s^{\alpha}\bar{T}(r,s)}{s^{\alpha}(1-\alpha)+\alpha}=\frac{1}{r}\frac{\partial}{\partial r}\left(r\frac{\partial\bar{T}(r,s)}{\partial r}\right)+\bar{Q}(r,s) \quad (28)$$

$$\frac{\partial\bar{u}(r,s)}{\partial r}\text{ and }\frac{\partial\bar{T}(r,s)}{\partial r}=0\text{ at }r=0\text{ for }s>0 \quad (29)$$

$$\bar{u}(r,s)=0\text{ and }\bar{T}(r,s)=0\text{ at }r=1\text{ for all }s>0 \quad (30)$$

Simplifying equations (27) and (28), we have

$$\frac{[s^{\alpha+1}(1-\alpha)+s\alpha+\lambda_1 s^{\alpha+1}]}{s^{\alpha}(1-\alpha)+\alpha}\bar{u}(r,s)=\frac{-[s^{\alpha}(1-\alpha)+\alpha]\bar{F}(s)-\lambda_1[s^{\alpha}\bar{F}(s)-s^{\alpha-1}f(0)]}{s^{\alpha}(1-\alpha)+\alpha}+\left[\frac{s^{\beta}(1-\beta)+\beta+\lambda_2 s^{\beta}}{s^{\beta}(1-\beta)+\beta}\right]\frac{1}{r}\frac{\partial}{\partial r}\left(r\frac{\partial\bar{u}(r,s)}{\partial r}\right) \quad (31)$$

$$\frac{Pr\lambda_1 s^{\alpha}\bar{T}(r,s)}{s^{\alpha}(1-\alpha)+\alpha}-\frac{1}{r}\frac{\partial}{\partial r}\left(r\frac{\partial\bar{T}(r,s)}{\partial r}\right)-\bar{Q}(r,s)=0 \quad (32)$$

Next, applying the finite Hankel transform (25) and using equations (29) and (30), we obtain

$$\frac{\left[[s^{\alpha+1}(1-\alpha)+s\alpha+\lambda_1 s^{\alpha+1}]\right]}{s^{\alpha}(1-\alpha)+\alpha}\bar{u}(\gamma_n,s)=\frac{-[s^{\alpha}(1-\alpha)+\alpha]\bar{F}(s)-\lambda_1[s^{\alpha}\bar{F}(s)-s^{\alpha-1}f(0)]}{s^{\alpha}(1-\alpha)+\alpha}\frac{J_1(\gamma_n)}{\gamma_n^2}-\gamma_n^2\overline{\left[\frac{s^{\beta}(1-\beta)+\beta+\lambda_2 s^{\beta}}{s^{\beta}(1-\beta)+\beta}\right]u}(\gamma_n,s) \quad (33)$$

$$\frac{Pr\lambda_1 s^{\alpha}}{s^{\alpha}(1-\alpha)+\alpha}\bar{T}(\gamma_n,s)+\gamma_n^2\bar{T}(\gamma_n,s)-\bar{Q}(r,s)\frac{J_1(\gamma_n)}{\gamma_n^2}=0 \quad (34)$$

Simplifying equations (33) and (34), we obtained

$$\bar{u}(\gamma_n,s)=\frac{-\{[s^{\beta}(1-\beta)+\beta][s^{\alpha}(1-\alpha)+\alpha][s^{\alpha}(1-\alpha)+\alpha]\bar{F}(s)-\lambda_1[s^{\alpha}\bar{F}(s)-s^{\alpha-1}f(0)]\}}{\{[s^{\beta}(1-\beta)+\beta][s^{\alpha+1}(1-\alpha)+s\alpha+\lambda_1 s^{\alpha+1}]\}+\gamma_n^2\{[s^{\beta}(1-\beta)+\beta+\lambda_2 s^{\beta}][s^{\alpha}(1-\alpha)+\alpha]\}}\frac{J_1(\gamma_n)}{\gamma_n^2} \quad (35)$$

$$\bar{T}(\gamma_n,s)=\left[\frac{s^{\alpha}(1-\alpha)+\alpha}{Pr\lambda_2 s^{\alpha}+\gamma_n^2(s^{\alpha}(1-\alpha)+\alpha)}\right]\bar{Q}(r,s)\frac{J_1(\gamma_n)}{\gamma_n^2} \quad (36)$$

Using the formulae (26), the inverse finite Hankel transforms for equations (35) and (36) are respectively given by:

$$\bar{u}(r,s)=2\sum_{n=1}^{\infty}\frac{J_0(\gamma_n r)}{J_0^2(\gamma_n)}$$

$$\left\{\frac{-\{[s^{\beta}(1-\beta)+\beta][s^{\alpha}(1-\alpha)+\alpha][s^{\alpha}(1-\alpha)+\alpha]\bar{F}(s)-\lambda_1[s^{\alpha}\bar{F}(s)-s^{\alpha-1}f(0)]\}}{\{[s^{\beta}(1-\beta)+\beta][s^{\alpha+1}(1-\alpha)+s\alpha+\lambda_1 s^{\alpha+1}]\}+\gamma_n^2\{[s^{\beta}(1-\beta)+\beta+\lambda_2 s^{\beta}][s^{\alpha}(1-\alpha)+\alpha]\}}\right\}\frac{J_1(\gamma_n)}{\gamma_n^2} \quad (37)$$

$$\bar{T}(r,s)=2\sum_{n=1}^{\infty}\frac{J_0(\gamma_n r)}{J_0^2(\gamma_n)}\left\{\left[\frac{s^{\alpha}(1-\alpha)+\alpha}{Pr\lambda_1 s^{\alpha}+\gamma_n^2(s^{\alpha}(1-\alpha)+\alpha)}\right]\bar{Q}(r,s)\right\}\frac{J_1(\gamma_n)}{\gamma_n^2} \quad (38)$$

Using the Stehfest's algorithm, the inverse Laplace transforms of equations (37) and (38) are given by

$$u(r,t)=\frac{\ln 2}{t}\sum_{j=1}^{2p}(-1)^{j+p}\sum_{i=\left[\frac{j+1}{2}\right]}^{Min(j,p)}\frac{i^p(2i)!}{i!(p-i)!(i-1)!(j-1)!(2i-j)!}\bar{u}\left(\frac{j\ln 2}{t}\right) \quad (39)$$

$$T(r,t)=\frac{\ln 2}{t}\sum_{j=1}^{2p}(-1)^{j+p}\sum_{i=\left[\frac{j+1}{2}\right]}^{Min(j,p)}\frac{i^p(2i)!}{i!(p-i)!(i-1)!(j-1)!(2i-j)!}\bar{T}\left(\frac{j\ln 2}{t}\right) \quad (40)$$

Equations (39) and (40) are the analytical solutions of Oldroyd-B fluid flow and heat transfer using Atangana-Baleanu fractional derivatives.

Skin Friction and Nusselt Number

Skin Friction (Surface Drag Force)

Skin friction is the resistive force exerted by a fluid on the surface of a body moving through it, or when fluid flows over a stationary body. It is primarily caused by the viscous effects within the boundary layer close to the surface of the object. Boundary Layer**:** A thin region near the surface where the velocity of the fluid changes from zero (due to the no-slip condition at the surface) to the free-stream velocity. Shear Stress($\boldsymbol{\tau_w}$)**:** The force per unit area acting parallel to the surface, which is a result of viscous forces in the boundary layer.

$$\tau_w=\mu\left(\frac{1+\lambda_2\,{}^{ABC}D_t^{\beta}}{1+\lambda_1\,{}^{ABC}D_t^{\alpha}}\right)\left(\frac{\partial u}{\partial r}\right)_{r=0} \quad (41)$$

Skin Friction Coefficient: The skin friction coefficient C_f is a dimensionless quantity that quantifies the ratio of the skin friction to the dynamic pressure of the fluid (Martín-Gil and Flores, 2024):

$$C_f=\frac{\tau_w}{\frac{1}{2}\rho u_m^2} \quad (42)$$

Nusselt Number (Heat Transfer Rate)

The Nusselt number (N_u) is a dimensionless number that quantifies the rate of convective heat transfer relative to the rate of conductive heat transfer within a fluid. It describes the enhancement of heat transfer through a fluid flow compared to pure conduction.

In the case of constant wall heat flux, the Nusselt number is generally defined as Zhao *et al.* (2024).

$$Nu=\frac{2q_w}{(T_w-T_b)k} \quad (43)$$

considering equation (14) (after dropping the * notation)

$$Nu=\frac{2}{(T_w-T_b)} \quad (44)$$

where T_b is the instantaneous bulk temperature at the wall defined by

$$T_b = \frac{\int_0^1 T\,u\,dr}{\int_0^1 u\,dr} \qquad (45)$$

Substituting equation (45) into equation (44) and using the boundary at $\left(T_w = \frac{11}{24}\right)$, we obtain

$$Nu = \frac{2}{\frac{11}{24} - \frac{\int_0^1 T\,u\,dr}{\int_0^1 u\,dr}} \qquad (46)$$

RESULT AND DISCUSSION

In order to obtain the physical interpretation of results regarding the behavior of the velocity and temperature at the variation of the fractional Oldroyd-B fluid, we carried out numerical simulation using MathCAD software and results were graphically presented in Figures 2 – 13. The result validation of the current work with previous work in the literature was presented in Figure 14.

Figures 2 and 3 are plotted, in order to present the evolution in time of the Maxwell fluid velocity for various fractional parameter α. The velocity diagrams have been sketched for small and large values time t, in Figures 2 and 3, respectively. The case of ordinary fluid corresponding to $\alpha = 1$ was, also, studied. It is observed from Figures 2 and 3, that in both cases, the influence of the fractional parameters on the fluid velocity is significant for the small values of the time t (t=0.1, 0.3, 0.5) in the particular case. Also, we must be noted that for higher values of the time t (t=0.7, 0.9, 1.0), the velocity variation with ordinary fluid is significantly higher than for fractional fluid.

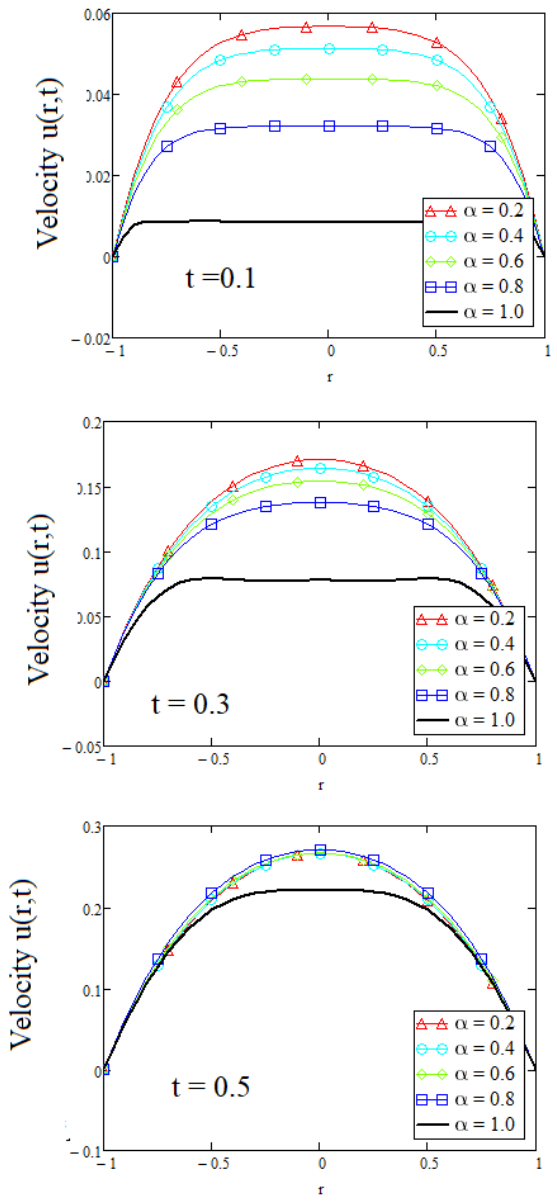

Figure 2: Velocity profile for small values of time t (t=0.1, 0.3, 0.5) and $\alpha_1 = 0.5$ with difference fractional parameter case of Maxwell fluid

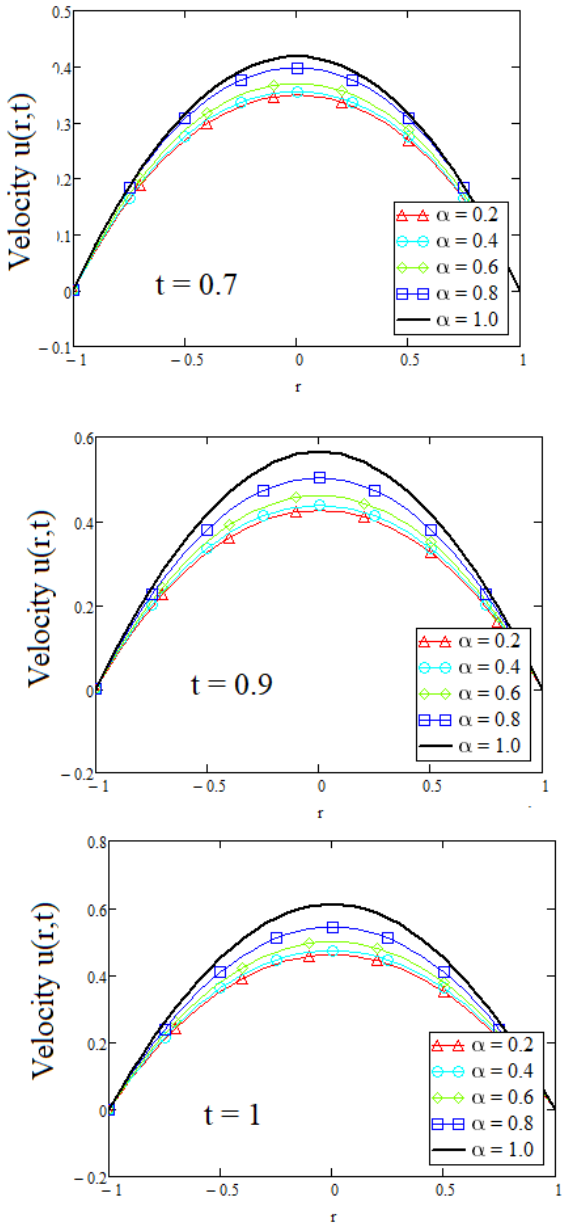

Figure 3: Velocity profile for large values of time t (t=0.7, 0.9, 1) and $\Lambda_1 = 0.5$ with difference fractional parameter case of Maxwell fluid

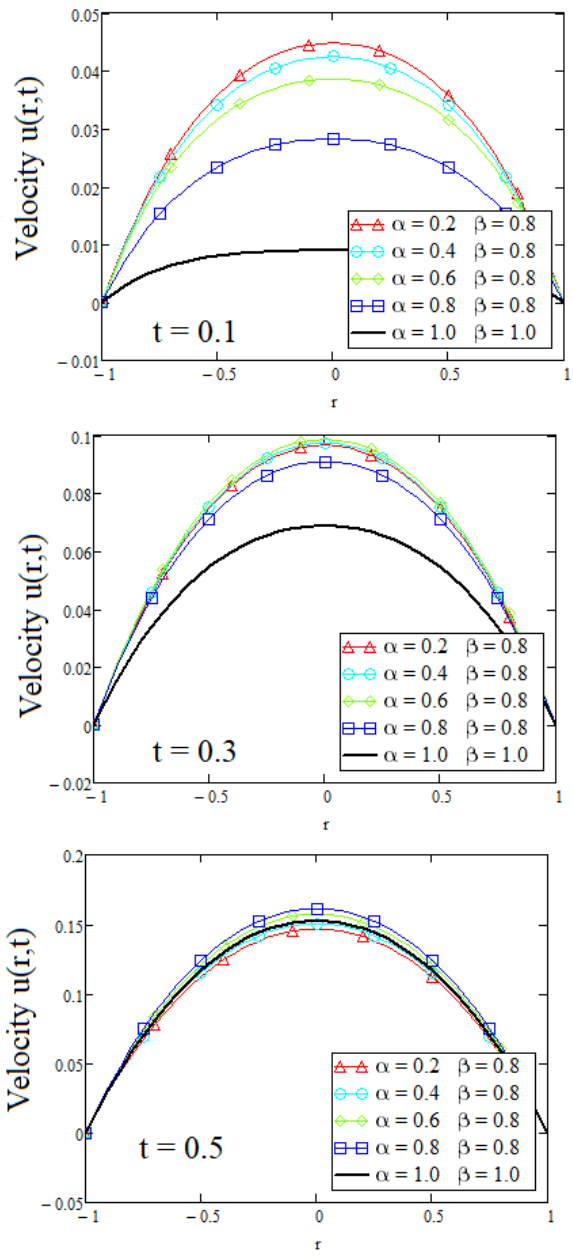

Figure 4: Velocity profile for small values of time t (t=0.1, 0.3, 0.5) $\Lambda_1 = 0.5, \Lambda_2 = 0.6$ with difference fractional parameter case of Oldroyd-B fluid

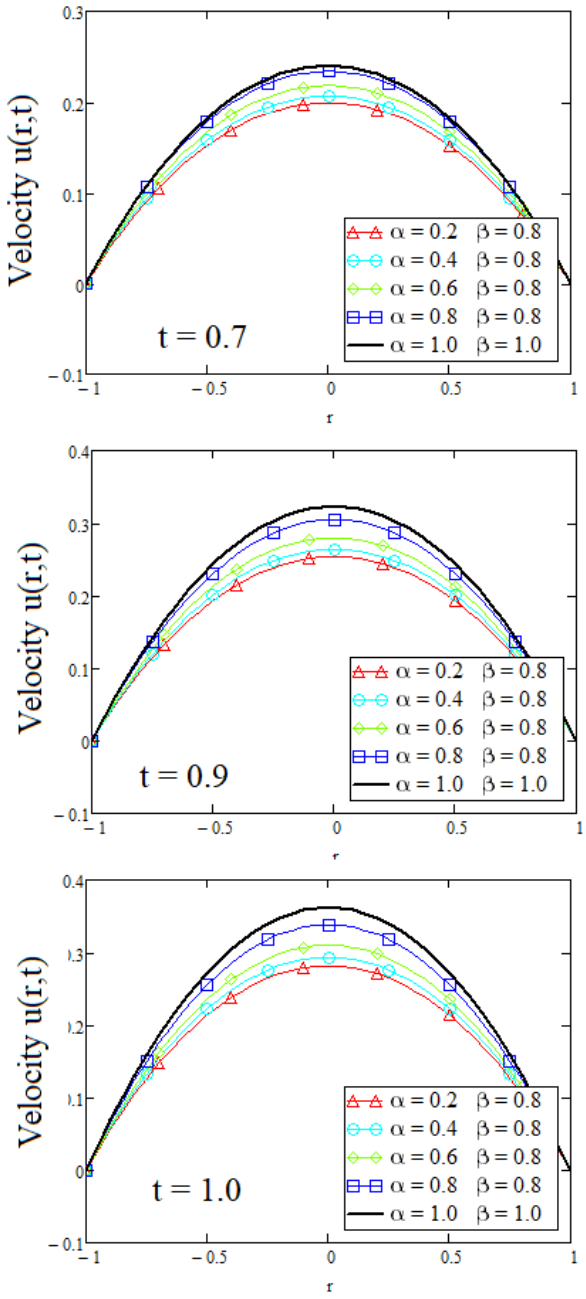

Figure 5: Velocity profile for large values of time t (t=0.7, 0.9, 1) and $\Lambda_1 = 0.5, \Lambda_2 = 0.6$ with difference fractional parameter case of Oldroyd-B fluid

Figures 4 and 5 are drawn in order to study the behavior of velocity with the radial coordinate r. In these figures we have considered the fractional parameters α and β in the relation $\alpha \leq \beta$for Figure and $\alpha \geq \beta$ for Figure 5. It is seen from these figures that there are values of time t and of the fractional parameters for which, the fractional fluid moves faster/slower than the ordinary fluid. The influence of fractional parameters on the fluid velocity is significant for small values of the time t. The reverse flow can produced at the motion beginning. The influence of memory effects, which are described by the time-fractional derivatives, is significantly in the case when the fractional parameters satisfy condition $\alpha < \beta$ and for small values of the time t.

Figures 6 and 7 illustrates the influence of pulsation frequency on the velocity profiles for fractional fluid $\alpha \leq \beta$, $\alpha \geq \beta$ and ordinary fluid ($\alpha = 1$ and $\beta = 1$). It can be found that the fluid velocity depends on the oscillating frequency and the fractional order form of the fluid. When the oscillating frequency increases, the amplitude of the wave form of the velocity profiles decreases, which is consistent with the case of ordinary fluids.

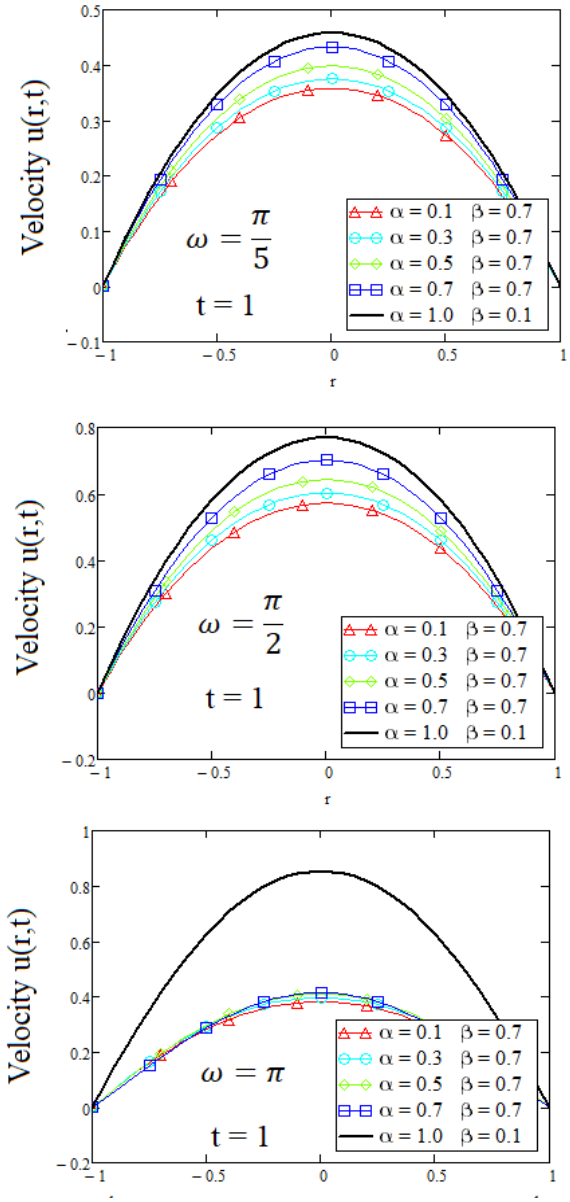

Figure 6: Velocity profile for different pulsation frequency $(\omega = \frac{\pi}{5}, \frac{\pi}{2}, \pi)$ and $\Lambda_1 = 0.5, \Lambda_2 = 0.6$ with difference fractional parameter α and β fixed; case of Oldroyd-B fluid

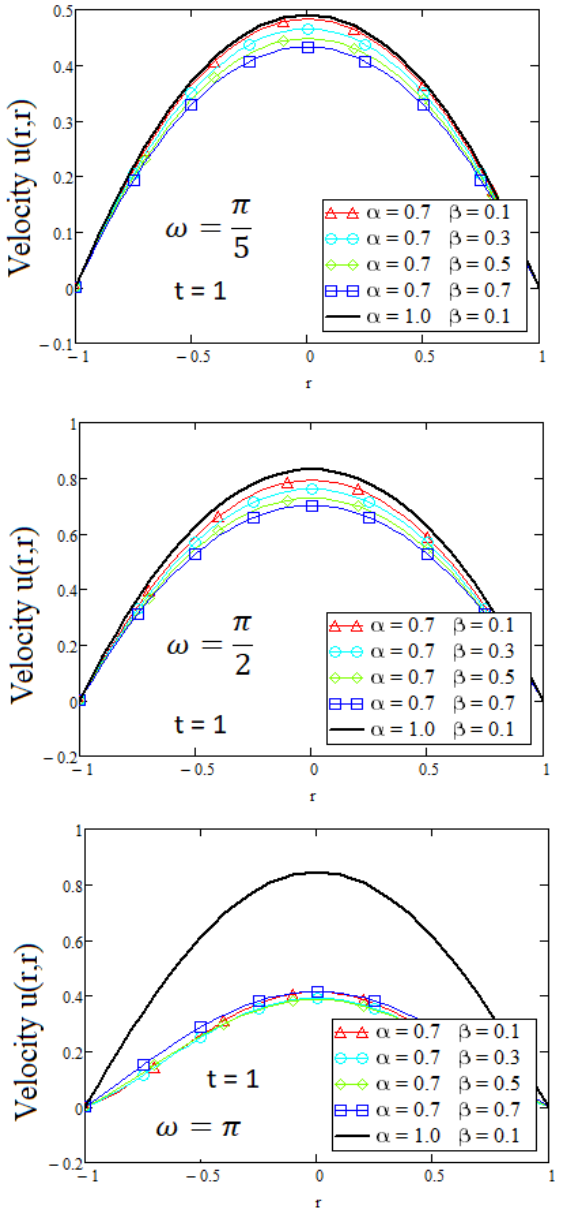

Figure 7: Velocity profile for different pulsation frequency $(\omega = \frac{\pi}{5}, \frac{\pi}{2}, \pi)$ and $\lambda_1 = 0.5, \lambda_2 = 0.6$ with difference fractional parameter β case of Oldroyd-B fluid

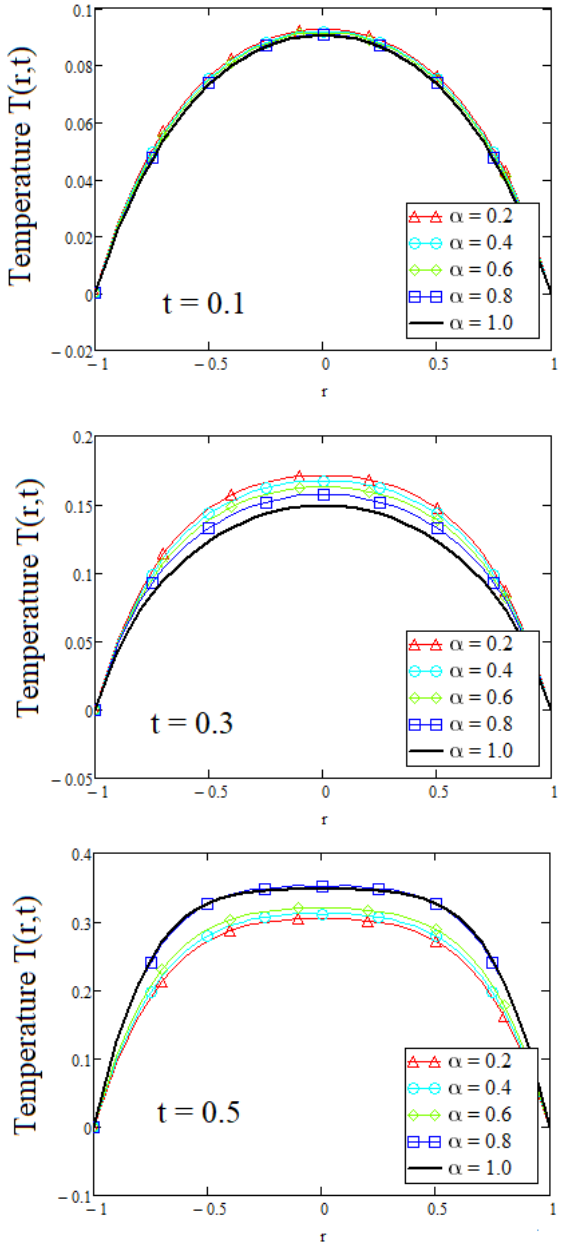

Figure 8: Temperature profile for small values of time t (t=0.1, 0.3, and 0.5) and $\lambda_1 = 0.5, \lambda_2 = 0$ with difference fractional parameter case of Maxwell fluid

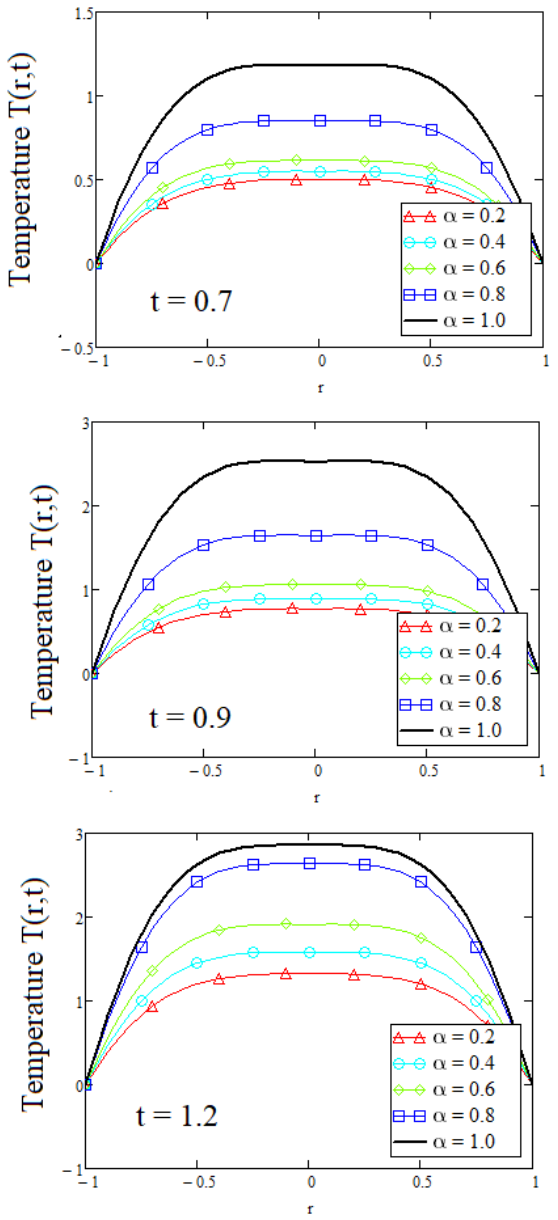

Figure 9: Temperature profile for large values of time t (t=0.7, 0.9, and 1.2) and $\Lambda_1 = 0.5, \Lambda_2 = 0$ with difference fractional parameter case of Maxwell fluid

Figures 8 and 9 were plotted in order to study the influence of fractional parameters α on the Maxwell fluid temperature distribution. The temperature distribution diagrams have been sketched for small values of time in Figure 8 and large values time in Figure 9. It is observed from Figures 8 and 9 that, the variation of the fractional parameters leads to decreasing of the fluid temperature as time progress. As the time progress, the temperature for the ordinary fluid is higher than fractional fluids.

Figures 10 and 11 illustrates the influence of fractional parameters α and β on the Oldroyd B fluid temperature distribution for fractional fluid $\alpha \leq \beta$, $\alpha \geq \beta$ and ordinary fluid ($\alpha = 1$ and $\beta = 1$). This behavior is similar to Maxwell except that higher temperature distribution was observed.

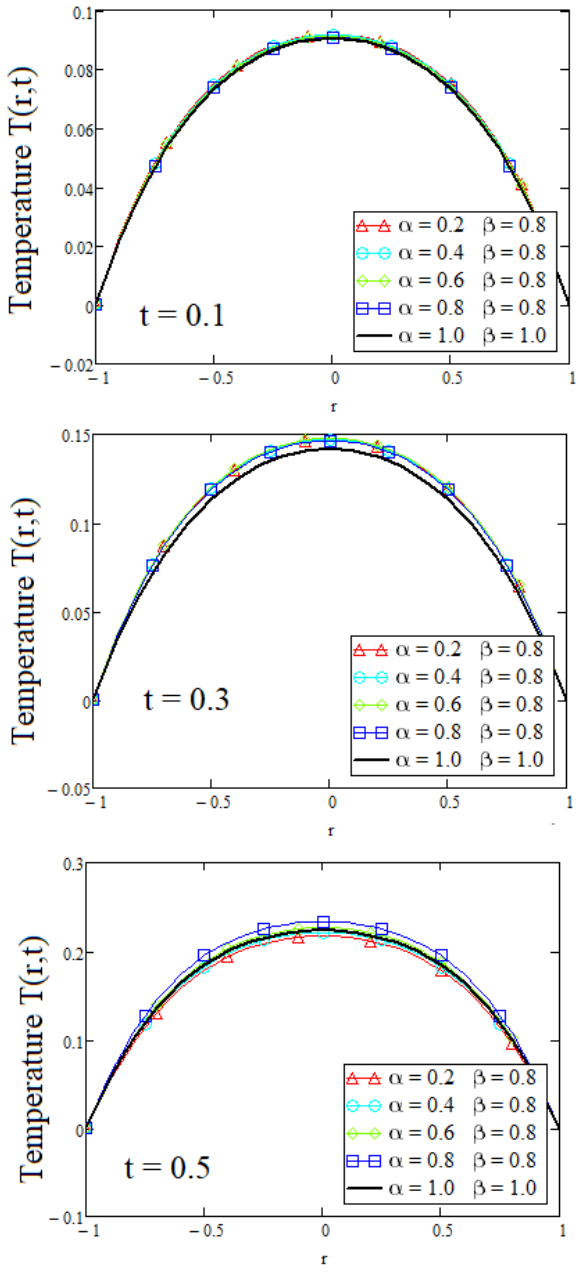

Figure 10: Temperature profile for small values of time t (t=0.1, 0.3, and 0.5) and $\Lambda_1 = 0.5, \Lambda_2 = 0.6$ with difference fractional parameter case of Oldroyd-B fluid

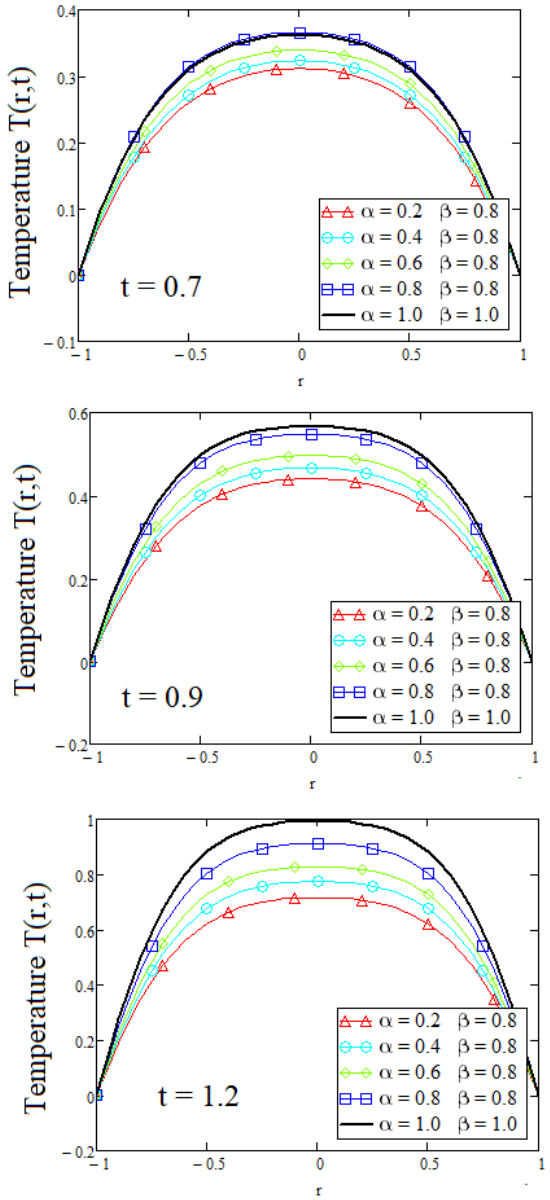

Figure 11: Temperature profile for large values of time t (t=0.7, 0.9, and 1.2) and $\Lambda_1 = 0.5, \Lambda_2 = 0.6$ with difference fractional parameter case of Oldroyd-B fluid

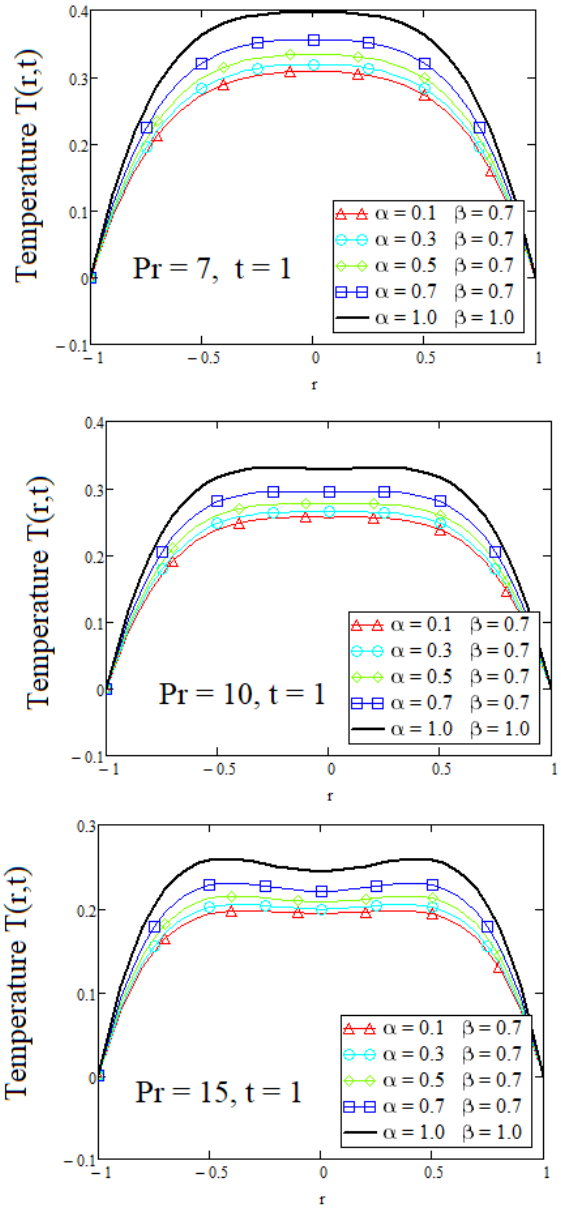

Figure 12: Temperature profile for different Prandtl number (Pr=7, 10, 15) and $\Lambda_1 = 0.5, \Lambda_2 = 0.6$ with difference fractional parameter α and β fixed. case of Oldroyd-B fluid

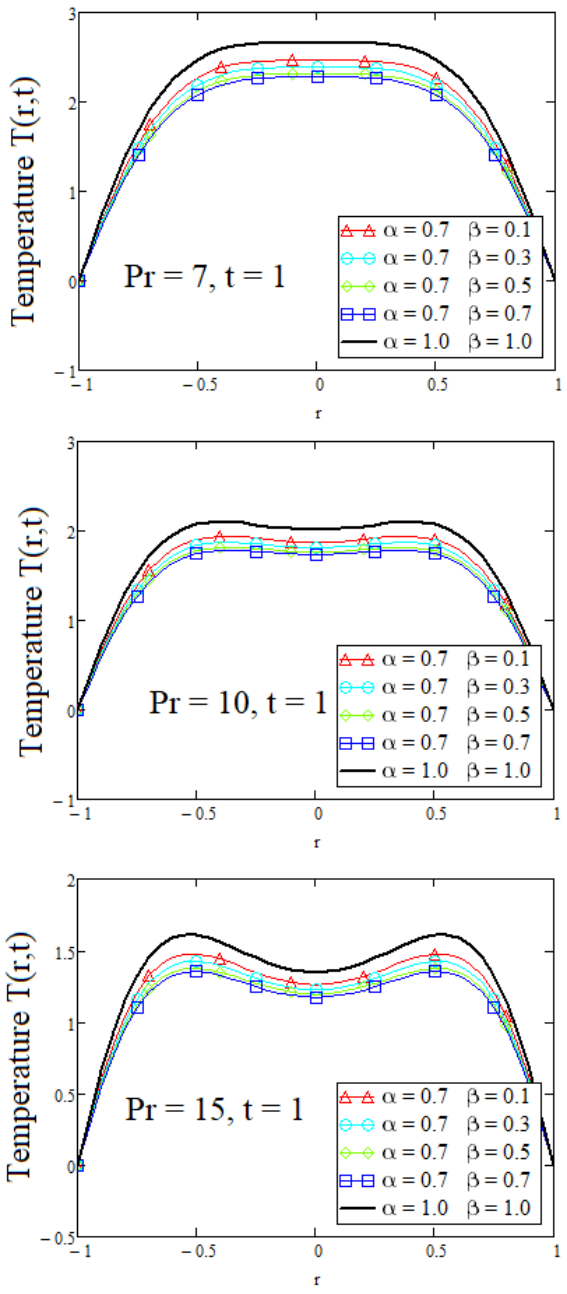

Figure 13: Temperature profile for different Prandtl number (Pr=7, 10, 15) and $\Lambda_1 = 0.5, \Lambda_2 = 0.6$ with difference fractional parameter β and α fixed. case of Oldroyd-B fluid

The influences of Prandtl number together with the fractional parameters on the temperature field were presented in Figures 12 and 13. In these figures we have considered the fractional parameters α and β in the relation $\alpha \leq \beta$ for Figure 12 and $\alpha \geq \beta$ for Figure 13. It noted that the fluid temperature is decreasing with the Prandtl number, but in Figure 13 $\alpha \geq \beta$, the temperature presents a slight increase.

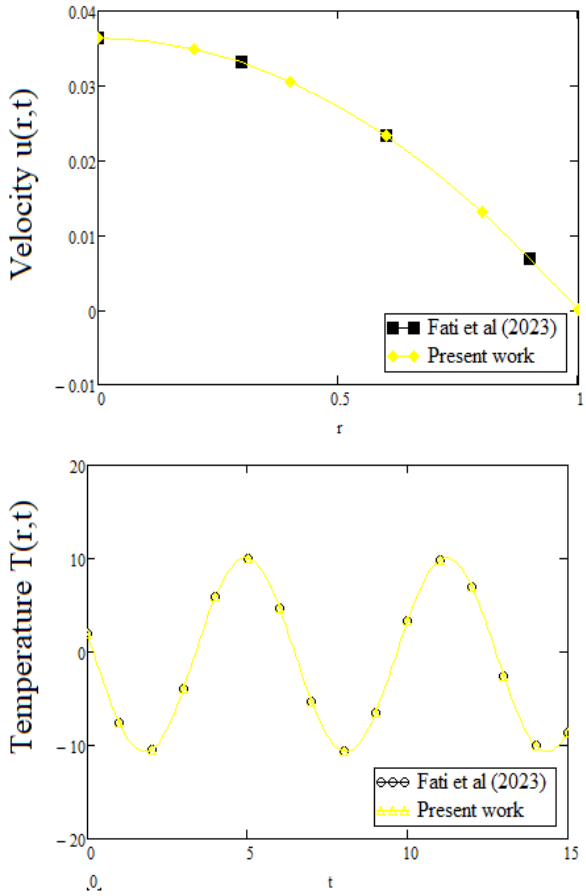

Figure 14: Comparison of results of velocity and Temperature distribution with the result of Fati *et al.* (2023) and present work

In Figure 14, the classical model solved by Fati *et al.* (2023) was compared with the fractional model (present work). It is clear from Figure 14, the result generated by Fati *et al.* (2023) for both velocity and temperature have the same agreement with present solution.

The important physical quantities, the local shear stress and local rate of heat transfer are respectively measured in terms of the local skin friction, C_f and the local Nusselt number, *Nu* and the numerical is as shown in Table 1 and 2.

Table 1: Numerical result of skin friction and Nusselt number the fractional parameters α and β in the relation $\alpha \geq \beta$

α	β	Λ_1	Λ_2	C_f	Nu
0.7	0.1	0.5	0.6	0.038841173217	1.1630
0.7	0.3	0.5	0.6	0.029843226489	1.45985
0.7	0.5	0.5	0.6	0.051369207540	0.43155
0.7	0.7	0.5	0.6	0.047224953021	0.7327
1	1	0.5	0.6	0.047110432048	0.8620

Table 2: Numerical result of skin friction and Nusselt number the fractional parameters α and β in the relation $\alpha \leq \beta$

α	β	λ_1	λ_2	C_f	Nu
0.1	0.7	0.5	0.6	0.029843226489	1.45985
0.3	0.7	0.5	0.6	0.029477381285	2.02355
0.5	0.7	0.5	0.6	0.029212566879	2.49065
0.7	0.7	0.5	0.6	0.028803221349	3.36493
1	1	0.5	0.6	0.028257391637	5.12438

Table 1 shows the skin friction C_f and the Nusselt number, Nu for different values of the fractional parameters α and β in the relation $\alpha \geq \beta$. The table shows that the skin friction C_f decreases with increase in the fractional parameter β for the fractional Oldroyd-B model between $\beta = 0.1, 0.3$ and the Nusselt number, Nu increases with increase in the fractional parameter in the same values of β. But, for $\beta = 0.5, 0.7$, the skin friction Cf decreases while the Nusselt number, Nu increases. Also the skin friction is minimal for β=1 which is a classical model of Oldroyd-B model and the Nusselt number Nu is also greatest for the classical Oldroyd-B model. Because of the minimal value of the skin friction C_f and the greatest heat transfer rate, the classical model of Oldroyd-B model are better working compared to the fractional Oldroyd-B model in flow and heat transfer.

Table 2 shows the skin friction C_f and the local Nusselt number, Nu with the different values of the fractional parameters α and β in the relation $\alpha \leq \beta$. It is observed that, the skin friction decreases with increase in the heat generation coefficient and the Nusselt number increases with increase in the heat generation parameter. Thus, high value of the heat generation parameter enhances high heat transfer. It also noted that for the classical model $\alpha = \beta = 1$, the fluid temperature observed lower of skin friction and higher value of Nusselt number.

CONCLUSION

Modeling and analytical solution of Oldroyd-B Atangana-Baleanu fractional time-fractional derivative in capillary tube were obtained for fluid velocity and temperature distribution by finite Hankel and Laplace transform methods. There are some main finds summarized in the follows:

(a) the physical obtained from simulation have illustrated the distinct behaviors of fractional order solutions when compared with classical model solutions.
(b) the fluid behavior of Maxwell fractional model have shown distinct behavior as compared to the Oldroyd-B fractional solution.
(c) the performance of fluid flow and heat transfer in capillary tube can be controlled by regulating the fractional order parameter.
(d) the influence of fractional fluid velocity is significant for the small values of the time, while for temperature distribution is significant for large values of time.
(e) the fluid velocity with fractional derivative moves faster/slower than the ordinary fluid.
(f) for large values of the Prandtl number, it is observed that the fluid temperature is decreasing, but in the middle of channel, the temperature presents a slight increase.
(g) the fluid temperature can be controlled by regulating Prandtl number and fractional parameters α and β

REFERENCES

Ali, M., Abdullahi, I., Yakubu, D. G., Adamu, G. T., Abdulhameed, M. and Baba, A. M. (2024). Transient MHD flow of fractional Burger's fluid model through a parallel microchannel with heat transfer and slip boundary condition. *Proceedings of the Institution of Mechanical Engineers, Part E: Journal of Process Mechanical Engineering*, 238(2), 774-787.

Altunkaya, A., Aydin, O. and Avci, M. (2023). Pulsating flow and heat transfer of power-law fluid in a circular pipe. *Nonlinear Analysis: Modelling and Control*, 28(1).

Anwar, T., Kumam, P., Khan, I. and Thounthong, P. (2022). Thermal analysis of MHD convective slip transport of fractional Oldroyd-B fluid over a plate. *Mechanics of Time-Dependent Materials*, 26(2), 431-462.

Dadheech, A., Sharma, S. and Al-Mdallal, Q. (2024). Numerical simulation for MHD Oldroyd-B fluid flow with melting and slip effect. *Scientific reports*, 14(1), 10591.

Fati, H. A., Abdulhameed, M. M., Adamu, M. Y. and Abdulhameed, B. M. (2023). Analytical solutions of non-Newtonian fluid flow and heat transfer over an oscillating capillary tube. *International Journal of Scientific Research in Mathematical and Statistical Sciences*, 10(76).

Guedri, K., Lashin, M. M., Abbasi, A., Khan, S. U., Tag-ElDin, E. S. M., Khan, M. I., ... and Galal, A. M. (2022). Modelling and mathematical investigation of blood-based flow of compressible rate type fluid with compressibility effects in a micro-channel. *Micro-machines*, 13(10), 1750.

Liu, T., Chen, T. and Miozzi, M. (2024). Correlation between skin friction and enstrophy convection velocity in near-wall turbulence. *European Journal of Mechanics-B/Fluids*, 104, 224-230.

Martín-Gil, A. and Flores, O. (2024). Predicting the skin friction's evolution in a forced turbulent channel flow. *Computers & Fluids*, 106417.

Quran, O., Olimat, A. N., Maaitah, H. and Duwairi, H. M. (2024). Computational influences of convection micropolar fluid influx and permeability on characteristics of heating rate and skin friction over vertical plate. *International Journal of Thermofluids*, 100885.

Rathore, N. and N, S. (2023). A modified thermal flux model to examine the enhanced heat transmission in hybrid blood flow through artery: A comparison between Maxwell and Oldroyd-B models. *Proceedings of the Institution of Mechanical Engineers, Part E: Journal of Process Mechanical Engineering*, 237(5), 1846-1853.

Sehra, S., Noor, A., Haq, S. U., Jan, S. U., Khan, I. and Mohamed, A. (2023). Heat transfer of generalized second grade fluid with MHD, radiation and exponential heating using Caputo–Fabrizio fractional derivatives approach. *Scientific Reports*, 13(1), 5220.

Sidahmed, A. O. (2024). Numerical study for MHD flow of an Oldroyd-B fluid over a stretching sheet in the presence of thermal radiation with Soret and Dufour effects. *International Journal of Analysis and Applications*, 22, 19-19.

Veltkamp, B., Jagielka, J., Velikov, K. P. and Bonn, D. (2023). Lubrication with non-Newtonian fluids. *Physical Review Applied*, 19(1), 014056.

Wang, X., Qiao, Y., Qi, H. and Xu, H. (2022). Numerical study of pulsatile non-Newtonian blood flow and heat transfer in small vessels under a magnetic field. *International Communications in Heat and Mass Transfer*, 133, 105930.

Yin D. and Ma H. B. (2013). Analytical solution of oscillating flow in a capillary tube, *International Journal of Heat and Mass Transfer*, 66, 699–705.

Zhao, Y., Fan, Y. and Li, W. (2024). Reynolds number effects on a velocity–vorticity correlation-based skin-friction drag decomposition in incompressible turbulent channel flows. *Journal of Fluid Mechanics*, 979, A20.